Inorg. Chem. **2004**, *43*, 4911–4920

Diruthenium Complexes $[\{(acac)_2Ru^{III}\}_2(\mu\text{-}OC_2H_5)_2]$, $[\{(acac)_2Ru^{III}\}_2(\mu\text{-L})](ClO_4)_2$, and $[\{(bpy)_2Ru^{II}\}_2(\mu\text{-L})](ClO_4)_4$ [L = $(NC_5H_4)_2$–N–C_6H_4–N–$(NC_5H_4)_2$, acac = Acetylacetonate, and bpy = 2,2′-Bipyridine]. Synthesis, Structure, Magnetic, Spectral, and Photophysical Aspects

Sanjib Kar,[†] Nripen Chanda,[†] Shaikh M. Mobin,[†] Anindya Datta,[†] Francisco A. Urbanos,[‡] Vedavati G. Puranik,[§] Reyes Jimenez-Aparicio,*[,‡] and Goutam Kumar Lahiri*[,†]

Department of Chemistry, Indian Institute of Technology-Bombay, Powai, Mumbai-400076, India, Departamento de Químicas Inorgánica, Facultad de Ciencias Químicas, Universidad Complutense, Ciudad Universitaria, E28040-Madrid, Spain, and Center for Materials Characterization, National Chemical Laboratory, Pune, Maharashtra-411008, India

Received January 28, 2004

Paramagnetic diruthenium(III) complexes $(acac)_2Ru^{III}(\mu\text{-}OC_2H_5)_2Ru^{III}(acac)_2$ (**6**) and $[(acac)_2Ru^{III}(\mu\text{-L})Ru^{III}(acac)_2](ClO_4)_2$, [**7**]$(ClO_4)_2$, were obtained via the reaction of binucleating bridging ligand, *N*,*N*,*N*′,*N*′-tetra(2-pyridyl)-1,4-phenylenediamine $[(NC_5H_4)_2\text{–N–}C_6H_4\text{–N-}(NC_5H_4)_2$, L] with the monomeric metal precursor unit $(acac)_2Ru^{II}(CH_3CN)_2$ in ethanol under aerobic conditions. However, the reaction of L with the metal fragment $Ru^{II}(bpy)_2(EtOH)_2^{2+}$ resulted in the corresponding $[(bpy)_2Ru^{II}(\mu\text{-L})Ru^{II}(bpy)_2](ClO_4)_4$, [**8**]$(ClO_4)_4$. Crystal structures of L and **6** show that, in each case, the asymmetric unit consists of two independent half-molecules. The Ru–Ru distances in the two crystallographically independent molecules (**F** and **G**) of **6** are found to be 2.6448(8) and 2.6515(8) Å, respectively. Variable-temperature magnetic studies suggest that the ruthenium(III) centers in **6** and [**7**]$(ClO_4)_2$ are very weakly antiferromagnetically coupled, having $J = -0.45$ and -0.63 cm^{-1}, respectively. The *g* value calculated for **6** by using the van Vleck equation turned out to be only 1.11, whereas for [**7**]$(ClO_4)_2$, the *g* value is 2.4, as expected for paramagnetic Ru(III) complexes. The paramagnetic complexes **6** and $[\mathbf{7}]^{2+}$ exhibit rhombic EPR spectra at 77 K in $CHCl_3$ ($g_1 = 2.420$, $g_2 = 2.192$, $g_3 = 1.710$ for **6** and $g_1 = 2.385$, $g_2 = 2.177$, $g_3 = 1.753$ for $[\mathbf{7}]^{2+}$). This indicates that **6** must have an intermolecular magnetic interaction, in fact, an antiferromagnetic interaction, along at least one of the crystal axes. This conclusion was supported by ZINDO/1-level calculations. The complexes **6**, $[\mathbf{7}]^{2+}$, and $[\mathbf{8}]^{4+}$ display closely spaced Ru(III)/Ru(II) couples with 70, 110, and 80 mV separations in potentials between the successive couples, respectively, implying weak intermetallic electrochemical coupling in their mixed-valent states. The electrochemical stability of the Ru(II) state follows the order: $[\mathbf{7}]^{2+} < \mathbf{6} < [\mathbf{8}]^{4+}$. The bipyridine derivative $[\mathbf{8}]^{4+}$ exhibits a strong luminescence [quantum yield (ϕ) = 0.18] at 600 nm in EtOH/MeOH (4:1) glass (at 77 K), with an estimated excited-state lifetime of approximately 10 μs.

Introduction

Although dioxo- (**A**) and dihydroxo- (**B**) bridged diruthenium cores have been extensively studied,[1] the investigation of the dialkoxo-bridged diruthenium core (**C**) has, to date, been confined to a limited number of complexes. These complexes are $[(bpy)_2Ru^{II}(\mu\text{-OR})_2Ru^{II}(bpy)_2]^{2+}$ (**1**),[2] $[(Cl_4Cat)_2Ru^{III}(\mu\text{-OR})_2Ru^{III}(Cl_4Cat)_2]^{4-}$ (**2a**)/$[(Cl_4Cat)_2Ru^{3.5+}(\mu\text{-OR})_2Ru^{3.5+}(Cl_4Cat)_2]^{3-}$ (**2b**),[3] mixed-valent $[\{Ru(bpy)\}_2(\mu\text{-OMe})_2(CO)(Cl)_3]$ (**3**),[4] $[(^tBuCN)_4Ru^{II}(\mu\text{-OR})_2Ru^{II}(CN^tBu)_4]^{2+}$

* To whom correspondence should be addressed. E-mail: lahiri@chem.iitb.ac.in.
[†] Indian Institute of Technology-Bombay.
[‡] Universidad Complutense.
[§] National Chemical Laboratory.

(1) (a) Power, J. M.; Evertz, K.; Henling, L.; Marsh, R.; Schaefer, W. P.; Labinger, J. A.; Bercaw, J. E. *Inorg. Chem.* **1990**, *29*, 5058. (b) Kelson, E. P.; Henling, L. M.; Schaefer, W. P.; Labinger, J. A.; Bercaw, J. E. *Inorg. Chem.* **1993**, *32*, 2863.

10.1021/ic0498900 CCC: $27.50
Published on Web 07/09/2004

(**4**),[5] and $[(\eta^5\text{-}C_5Me_5)\ Ru^{II}(\mu\text{-}OMe)]_2/[(\eta^5\text{-}C_5Me_5)(CO)Ru^{II}(\mu\text{-}OEt)]_2$ (**5**)[6] (bpy = 2,2′-bipyridine, Cl_4Cat = tetrachlorocatecholate).

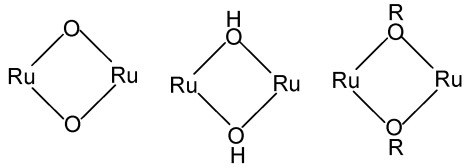

A **B** **C**

Complexes **2a** and **2b** were reported to be the ruthenium−ruthenium-bonded dialkoxo-bridged species. However, these were selectively obtained from the metal−metal-bonded precursor complex $Na_3[Ru_2(Cl_4Cat)_4\cdot THF]$.[3,7] The ruthenium(III) centers in **2a** are magnetically coupled to provide a diamagnetic ground state, whereas **2b** is a paramagnetic species with a doublet ground state.

The present article demonstrates the formation of a paramagnetic dialkoxo-bridged diruthenium core of type **C**, $[(acac)_2Ru^{III}(\mu\text{-}OC_2H_5)_2Ru^{III}(acac)_2]$ (**6**), and *N*,*N*,*N*′,*N*′-tetra(2-pyridyl)-1,4-phenylenediamine- (L) bridged paramagnetic and diamagnetic diruthenium complexes $[(acac)_2Ru^{III}(\mu\text{-}L)Ru^{III}(acac)_2](ClO_4)_2$, [**7**]$(ClO_4)_2$, and $[(bpy)_2Ru^{II}(\mu\text{-}L)Ru^{II}(bpy)_2](ClO_4)_4$, [**8**]$(ClO_4)_4$, respectively. The synthesis of L and the aspects of its metalation with platinum and lanthanides have been explored recently.[8] Also, the discrete metal−metal-bonded Ru_2^{6+} unit has proven to be elusive until recently,[3,9] although a large number of complexes of type Ru_2^{n+} (n = 4, 5) are known.[10]

In this paper, we report the synthesis of **6**, [**7**]$(ClO_4)_2$, and [**8**]$(ClO_4)_4$ and examine the crystal structures of L and **6**. We also investigate the spectroscopic, magnetic, and electrochemical properties of these species; perform ZINDO/1-level calculations to confirm the magnetic data on **6**; and investigate certain photophysical aspects of [**8**]$(ClO_4)_4$.

Results and Discussion

Synthesis and Characterization. The reaction of a potentially binucleating ligand, *N*,*N*,*N*′,*N*′-tetra(2-pyridyl)-1,4-phenylenediamine $[(NC_5H_4)_2{-}N{-}C_6H_4{-}N{-}(NC_5H_4)_2$, L] with the precursor monomeric unit $(acac)_2Ru^{II}(CH_3CN)_2$ in a 1:2 molar ratio in boiling ethanol under aerobic conditions followed by chromatographic purification of the crude product using a silica gel column resulted in paramagnetic complexes $[(acac)_2Ru^{III}(\mu\text{-}OC_2H_5)_2Ru^{III}(acac)_2]$ (**6**) and $[(acac)_2Ru^{III}(\mu\text{-L})Ru^{III}(acac)_2](ClO_4)_2$, [**7**]$(ClO_4)_2$ (Scheme 1). When the same reaction was carried out under a dinitrogen atmosphere followed by chromatographic purification of the crude product using a silica gel column, the complex [**7**]$(ClO_4)_2$ was isolated as a major product (75%), along with a slight amount of complex **6** (3−5%). Thus, during the reaction process (Scheme 1) and, in the case of the nitrogen reaction, specifically during the chromatographic process, the ruthenium ion is oxidized from its starting bivalent state in $(acac)_2Ru^{II}(CH_3CN)_2$ to the trivalent state in **6** and [**7**]$(ClO_4)_2$. The oxygen in air is the probable oxidant (see later). Because the bridging ligand L or any fragment of L is not present in **6**, the reaction of $(acac)_2Ru^{II}(CH_3CN)_2$ in only ethanol or in EtOH/$NaOC_2H_5$ or EtOH/KOH was also tested under identical reaction conditions as stated in Scheme 1 but in the absence of L. However, the desired product **6** was not obtained, even though the other corresponding dialkoxo-bridged diruthenium complexes (**1**−**5**) were prepared by following the methods just stated above.[2−6] As the reaction takes place particularly under thermal conditions, the pure products are obtained after chromatographic operations, and more importantly, we do not observe any stable intermediate, it is difficult at present to draw any conclusion regarding the specific role of L in facilitating the formation of **6**. However, the above control experiments probably suggest that the reaction initially proceeds through the binding of L with the $\{Ru(acac)_2\}$ moiety, followed by its subsequent transformation to the product **6**. In contrast, the reaction of $Ru^{II}(bpy)_2(EtOH)_2^{2+}$ with L under the reaction conditions stated in Scheme 1 resulted in the expected dinuclear product $[(bpy)_2Ru^{II}(\mu\text{-L})Ru^{II}(bpy)_2](ClO_4)_4$, [**8**]$(ClO_4)_4$. Thus, the formation of dialkoxo-bridged complex **6** is sensitive to the nature of the terminal ligand.

The complexes exhibit satisfactory elemental analysis, and the species [**7**]$(ClO_4)_2$ and [**8**]$(ClO_4)_4$ show 1:2 and 1:4 conductivities, respectively, in acetonitrile (see the Experimental Section). The formation of the complexes was confirmed by their electrospray mass spectra in acetonitrile. Thus, complexes **6**, [**7**]$(ClO_4)_2$ and [**8**]$(ClO_4)_4$ show maximum molecular ion peaks (m/z) at 688.82, 1115.09, and 1542.19, respectively, corresponding to $[\mathbf{6}]^+$ (calculated molecular weight = 688.70), $\{[\mathbf{7}](ClO_4)\}^+$ (calculated molecular weight = 1115.11), and $\{[\mathbf{8}](ClO_4)_3\}^+$ (calculated molecular weight = 1542), as reported in the Supporting

(2) (a) Bardwell, D.; Jeffery, J. C.; Joulie, L.; Ward, M. D. *J. Chem. Soc., Dalton Trans.* **1993**, 2255. (b) Bardwell, D.; Horsburgh, L.; Jeffery, J. C.; Joulie, L. F.; Ward, M. D.; Webster, I.; Yellowlees, L. J. *J. Chem. Soc., Dalton Trans.* **1996**, 2527.
(3) Miyasaka, H.; Chang, H.-C.; Mochizuki, K.; Kitagawa, S. *Inorg. Chem.* **2001**, *40*, 3544.
(4) Eskelinen, E.; Kinnunen, T.-J. J.; Haukka, M.; Pakkanen, T. A. *Eur. J. Inorg. Chem.* **2002**, 1169.
(5) Chalmers, A. A.; Liles, D. C.; Meintjies, E.; Oosthuizen, H. E.; Pretorius, J. A.; Singleton, E. *J. Chem. Soc., Chem. Commun*. **1985**, 1340.
(6) Loren, S. D.; Campion, B. K.; Heyn, R. H.; Tilley, T. D.; Bursten, B. E.; Luth, K. W. *J. Am. Chem. Soc.* **1989**, *111*, 4712.
(7) Kondo, M.; Hamatani, M.; Kitagawa, S.; Pierpont, C. G.; Unoura, K. *J. Am. Chem. Soc*. **1998**, *120*, 455.
(8) (a) Liu, Q.-D.; Jia, W.-L.; Wu, G.; Wang, S. *Organometallics* **2003**, *22*, 3781. (b) Yang, W.-Y.; Chen, L.; Wang, S. *Inorg. Chem*. **2001**, *40*, 507.
(9) (a) Cotton, F. A.; Yokochi, A. *Inorg. Chem*. **1997**, *36*, 567. (b) Zhilyaev, A. N.; Fomina, T. A.; Kuzmenko, I. V.; Rotov, A. V.; Baranovskii, I. B. *Russ. J. Inorg. Chem.* (*Engl. Transl.*) **1989**, *34*, 532. (c) Kuzmenko, I. V.; Zhilyaev, A. N.; Fomina, T. A.; Porai-Koshits, M. A.; Baranovskii, I. B. *Russ. J. Inorg. Chem.* (*Engl. Transl.*) **1989**, *34*, 1457. (d) Cotton, F. A.; Datta, T.; Labella, L.; Shang, M. *Inorg. Chim. Acta* **1993**, *203*, 55. (e) Bear, J. L.; Han, B. C.; Huang, S. R. *J. Am.Chem. Soc*. **1993**, *115*, 1175. (f) Li, Y. L.; Han, B. C.; Bear, J. L.; Kadish, K. M. *Inorg. Chem*. **1993**, *32*, 4175. (g) Bear, J. L.; Li, Y.; Han, B.; Kadish, K. M. *Inorg. Chem*. **1996**, *35*, 1395. (h) Bear, J. L.; Li, Y.; Han, B.; Caemelbecke, E. V.; Kadish, K. M. *Inorg. Chem*. **1997**, *36*, 5449. (i) Bear, J. L.; Li, Y.; Han, B.; Caemelbecke, E. V.; Kadish, K. M. *Inorg. Chem.* **2001**, *40*, 182. (j) Xu, G.-L.; Jablonski, C. G.; Ren, T. *Inorg. Chim. Acta* **2003**, *343*, 387. (k) Chen, W. Z.; Ren, T. *Inorg. Chem*. **2003**, *42*, 8847.
(10) Cotton, F. A.; Walton, R. A. *Multiple Bonds between Metal Atoms*, 2nd ed.; Oxford University Press: Oxford, U.K., 1993.

Scheme 1. (i) EtOH, Δ

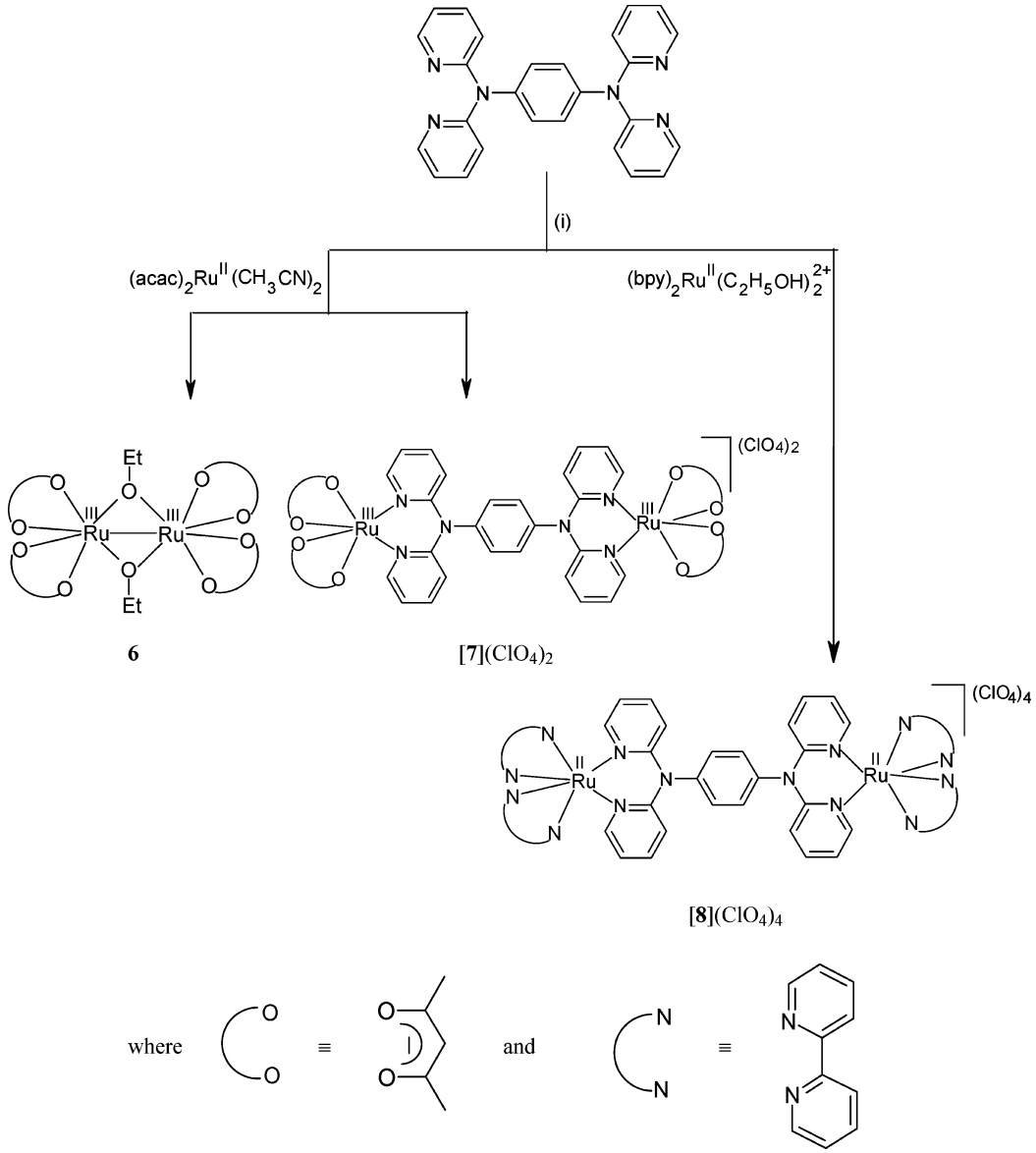

Information (Figures S1−S3). The ^{1}H NMR spectrum of the free ligand (L) in $CDCl_3$ [δ, ppm (J, Hz): d, 8.34 (5.3); t, 7.60 (9.1, 7.8); s, 7.19; d, 7.09 (8.4); t, 6.95 (6.2, 5.8)] matches well with the reported data.[8b] The ^{1}H NMR spectrum of the diamagnetic complex [**8**]$(ClO_4)_4$ exhibits a calculated number of 13 partially overlapping signals corresponding to one-fourth of the molecule (Supporting Information, Figure S4).

Crystal Structures. The crystal structure of the free ligand is shown in the Supporting Information (Figure S5). The asymmetric unit contains two crystallographically independent molecules (**D** and **E**), both having inversion centers. Bond distances and angles (Supporting Information, Table S1) agree well with the standard reported data.[11] Important crystallographic data are summarized in Table 1.

Table 1. Crystallographic Data for L and **6**

	L	**6**
molecular formula	$C_{26}H_{20}N_6$	$C_{24}H_{38}O_{10}Ru_2$
formula weight	416.48	688.68
radiation	Mo Kα	Mo Kα
crystal symmetry	monoclinic	monoclinic
space group	*C*2/*c*	*P*21/*c*
a (Å)	26.665(2)	10.4400(10)
b (Å)	10.1990(13)	17.8600(16)
c (Å)	16.3230(16)	15.9120(14)
β (deg)	105.200(7)	102.603(8)
V (Å^3)	4283.8(8)	2895.4(5)
Z	8	4
μ (mm^{-1})	0.080	1.092
T (K)	293(2)	293(2)
D_{calcd} (g cm^{-3})	1.292	1.580
2θ range (deg)	3.16−49.9	3.46−49.84
e data (R_{int})	2546(0.000)	3232(0.000)
R1 [$I > 2\sigma(I)$]	0.0636	0.0293
wR2 (all data)	0.1175	0.0743
GOF	1.068	1.058

The crystal structure of complex **6** is shown in Figure 1. The asymmetric unit consists of two independent half-

(11) (a) Mondal, B.; Puranik, V. G.; Lahiri, G. K. *Inorg. Chem.* **2002**, *41*, 5831. (b) Chanda, N.; Mondal, B.; Puranik, V. G.; Lahiri, G. K. *Polyhedron* **2002**, *21* 2033. (c) Mondal, B.; Lahiri, G. K.; Naumov, P.; Ng, S. W. *J. Mol. Struct.* **2002**, *613*, 131. (d) Chakraborty, S.; Laye, R. H.; Paul, R. L.; Gonnade, R. G.; Puranik, V. G.; Ward, M. D.; Lahiri, G. K. *J. Chem. Soc., Dalton Trans.* **2002**, 1172.

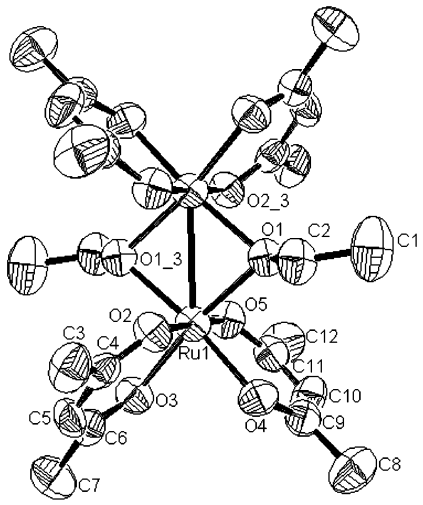

F

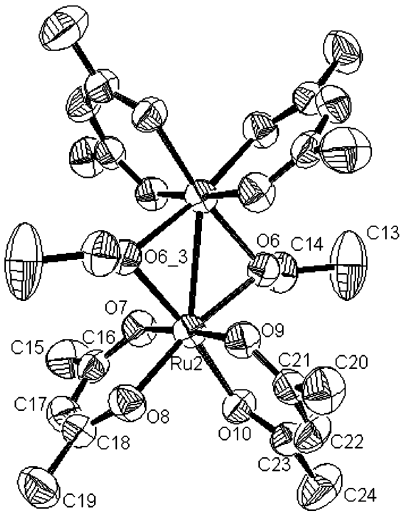

G

Figure 1. ORTEP diagram of $[(acac)_2Ru^{III}(\mu\text{-}OC_2H_5)_2Ru^{III}(acac)_2]$ (**6**).

Table 2. Selected Bond Distances (Å) and Angles (deg) for $[(acac)_2Ru^{III}(\mu\text{-}OC_2H_5)_2Ru^{III}(acac)_2]$, **6**

F		**G**	
Ru(1)−O(1)	2.024(3)	Ru(2)−O(6)	2.026(3)
Ru(1)−O(2)	2.038(4)	Ru(2)−O(7)	2.039(3)
Ru(1)−O(3)	2.013(4)	Ru(2)−O(8)	2.003(3)
Ru(1)−O(4)	2.007(3)	Ru(2)−O(9)	2.030(3)
Ru(1)−O(5)	2.045(3)	Ru(2)−O(10)	2.000(4)
Ru(1)−Ru(1)#1	2.6448(8)	Ru(2)−Ru(2)#2	2.6515(8)
O(2)−C(4)	1.241(7)	O(7)−C(16)	1.262(6)
C(3)−C(4)	1.513(9)	C(15)−C(16)	1.504(8)
C(4)−C(5)	1.410(8)	C(16)−C(17)	1.398(7)
C(5)−C(6)	1.391(8)	C(17)−C(18)	1.373(8)
C(6)−C(7)	1.486(10)	C(18)−C(19)	1.504(8)
O(3)−C(6)	1.286(7)	O(8)−C(18)	1.280(6)
O(4)−C(9)	1.273(6)	O(10)−C(23)	1.275(6)
C(8)−C(9)	1.500(9)	C(23)−C(24)	1.500(10)
C(9)−C(10)	1.386(8)	C(22)−C(23)	1.381(8)
C(10)−C(11)	1.385(8)	C(21)−C(22)	1.388(8)
C(11)−C(12)	1.504(9)	C(20)−C(21)	1.505(8)
O(5)−C(11)	1.263(6)	O(9)−C(21)	1.251(6)
O(1)−C(2)	1.444(6)	O(6)−C(14)	1.444(6)
C(1)−C(2)	1.447(11)	C(13)−C(14)	1.426(12)
O(4)−Ru(1)−O(3)	87.02(15)	O(10)−Ru(2)−O(8)	86.88(14)
O(4)−Ru(1)−O(1)	86.25(14)	O(10)−Ru(2)−O(6)	87.35(13)
O(3)−Ru(1)−O(1)	170.91(15)	O(8)−Ru(2)−O(6)	169.49(14)
O(4)−Ru(1)−O(2)	86.98(14)	O(10)−Ru(2)−O(9)	93.40(16)
O(3)−Ru(1)−O(2)	93.39(18)	O(8)−Ru(2)−O(9)	83.42(13)
O(1)−Ru(1)−O(2)	92.35(15)	O(6)−Ru(2)−O(9)	88.16(12)
O(4)−Ru(1)−O(5)	92.65(14)	O(10)−Ru(2)−O(7)	84.49(14)
O(3)−Ru(1)−O(5)	84.06(16)	O(8)−Ru(2)−O(7)	93.56(14)
O(1)−Ru(1)−O(5)	90.15(14)	O(6)−Ru(2)−O(7)	94.62(13)
O(2)−Ru(1)−O(5)	177.44(16)	O(9)−Ru(2)−O(7)	176.42(13)

molecules (**F** and **G**). The bond distances and angles in the two independent half-molecules were found to be slightly different (Table 2), which is presumably due to the effect of crystal packing forces. The Ru−O(acac) distances[12] involving oxygen atoms trans to the alkoxide groups [average = 2.010(4) Å in **F**, and average = 2.001(4) Å in **G**] are discernibly shorter than those involving oxygen atoms cis to the alkoxide groups [average = 2.041(4) Å in **F,** and average = 2.038(3) Å) in **G**]. The Ru^{III}−O (alkoxide) bond distances [average = 2.024(3) Å] and Ru−$(\mu$-OEt$)_2$−Ru angles [average = 81.64(12)°] in **6** are comparable to those of the related complex **2a**.[3] The Ru^{III}−Ru^{III} bond distances in **F** and **G** were found to be 2.6448(8) and 2.6515(8) Å, respectively. These are slightly longer than the distance 2.628(2) Å reported for the similar but diamagnetic complex $[(Cl_4Cat)_2Ru^{III}(\mu\text{-}OEt)_2Ru^{III}(Cl_4Cat)_2]^{4-}$ (**2a**).[3] Although the bond distances and bond angles in complex **6** are comparable to those described for compound **2a**, the magnetic properties are observed to be quite different (see later). These complexes have similar molecular structures, and the Ru−Ru bond length is only slightly longer in **6** than in compound **2a**. The configuration $\sigma^2\pi^2\delta^{*2}\delta^2\pi^{*2}$ was proposed for complex **2a**, similarly to other edge-sharing bioctahedral complexes.[13] In this configuration, only one π^* level exists, and therefore, these diruthenium(III) complexes must be diamagnetic. This is consistent with the magnetic behavior observed in complex **2a**.[3] However, compound **6** is paramagnetic, with a magnetic moment at room temperature close to that for the presence of two unpaired electrons per dinuclear unit (see later). This clearly indicates that the interaction between the Ru(III) centers in **6**, at room temperature, is very weak despite the structural similarity with complex **2a**. The magnetic data suggest that, in this complex (**6**), there is no metal−metal bond; rather, a weak interaction persists. It should be noted that, similarly to complex **2a,** the diamagnetic dihydroxo-bridged diruthenium(III) complex $[(L_{OMe})(CH_3CN)Ru^{III}(\mu\text{-}OH)_2Ru^{III}(CH_3CN)(L_{OMe})][CF_3SO_3]_2$ (L_{OMe} = $[(\eta^5\text{-}C_5H_5)\text{-}Co\{P(O)(OCH_3)_2\}_3]^-$) exhibited a Ru−Ru single bond distance of 2.622(1) Å.[1b] Similarly, the diamagnetic dioxo-bridged diruthenium(IV) complexes $[(L_{OEt})(H_2O)Ru^{IV}(\mu\text{-}O)_2\text{-}Ru^{IV}(H_2O)(L_{OEt})][CF_3SO_3]_2$ and $[(L_{OEt})(HO)Ru^{IV}(\mu\text{-}O)_2Ru^{IV}\text{-}(OH)(L_{OEt})]$ (L_{OEt} = $[(\eta^5\text{-}C_5H_5)Co\{P(O)(OEt)_2\}_3]^-$) showed

(12) Chao, G. K. J.; Sime, R. L.; Sime, R. J. *Acta Crystallogr*. **1973**, *B29*, 2845.

(13) (a) Shaik, S.; Hoffmann, R.; Fisel, C. R.; Summervill, R. H. *J. Am. Chem. Soc.* **1980**, *102*, 4555. (b) Cotton, F. A.; Wilkinson, G.; Murillo, C. A.; Bochmann, M. *Advanced Inorganic Chemistry*, 6th ed.; Wiley: New York, 2003: p 648.

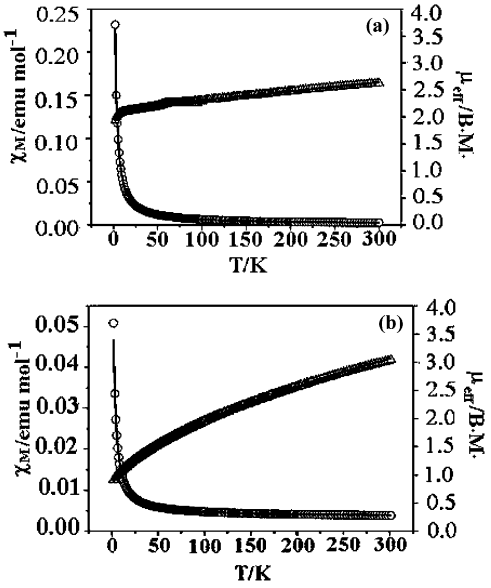

Figure 2. Plots of magnetic susceptibility and magnetic moment versus temperature for (a) $[(acac)_2Ru^{III}(\mu\text{-L})Ru^{III}(acac)_2](ClO_4)_2$, [**7**]$(ClO_4)_2$, and (b) $[(acac)_2Ru^{III}(\mu\text{-}OC_2H_5)_2Ru^{III}(acac)_2]$, **6**.

ruthenium−ruthenium double bond distances of 2.505(1) and 2.452(1) Å, respectively.[1a]

Packing diagrams of **6** (Supporting Information, Figure S6) show that the metal atoms lie in a chain along the crystallographic *b* and *c* axes, whereas they are seen as discrete entities along the *a* axis.

Magnetic Behavior. (a) Magnetic Moment. The compound [**8**]$(ClO_4)_4$ is diamagnetic. This is also expected, as each low-spin ruthenium(II) ion has an almost octahedral environment.

The paramagnetic dinuclear complex bridged by L, [**7**]-$(ClO_4)_2$, has a magnetic moment (per dinuclear unit) of 2.63 μ_B at 300 K that drops to 1.93 μ_B at 2 K. The variation of magnetic susceptibility with temperature shows typical paramagnetic behavior (Figure 2a). The model used to fit the magnetic data considers a general isotropic exchange spin Hamiltonian $H = -2J\mathbf{S}_1\cdot\mathbf{S}_2$, where $\mathbf{S}_1 = \mathbf{S}_2 = {}^1/_2$, using the van Vleck equation (eq 1)[14]

$$\chi_M = \frac{Ng^2\beta^2}{3kT}\frac{1}{1 + {}^1/_3\exp(-2J/kT)} + \mathrm{TIP} \qquad (1)$$

The parameter values obtained are $g = 2.4$, $J = -0.45$ cm^{-1}, and TIP $= 1 \times 10^{-3}$ cm^3/mol, with the quality of the fit given by $\sigma^2 = 1.99 \times 10^{-5}$. This *g* value is consistent with those observed in other mononuclear Ru(III) and dinuclear Ru(II)−Ru(III) complexes.[15] The low and negative *J* value indicates a very weak intramolecular antiferromagnetic coupling between the unpaired electrons of the Ru(III) centers of each dinuclear molecule.

Alternatively, it is possible to fit magnetic data using eq 2

$$\chi_M = \frac{C}{T - \theta} + TIP \qquad (2)$$

However, eq 2, used to fit the magnetic data of some mononuclear low-spin Ru(III) complexes, cannot be utilized for complexes **6** and [**7**]$(ClO_4)_2$, because the representations of $1/\chi_M$ versus temperature for these complexes are not linear in any range of temperature between 2 and 300 K (Supporting Information, Figure S7). Nevertheless, eq 2 will prove useful later, in providing valuable information on the intermolecular coupling.

Complex **6** has a similar magnetic behavior, showing a magnetic moment of 3.03 μ_B (per dinuclear unit) at 300 K that drops to 0.78 μ_B at 2 K (Figure 2b). All attempts to fit the experimental data using eq 1 stated above give anomalous *g* values lower than 2.[16] For example, the best fit using the van Vleck equation leads to the following values: $g = 1.11$, $J = -0.63$ cm^{-1}, TIP $= 3.4 \times 10^{-3}$ cm^3/mol, with a quality of fit of $\sigma^2 = 3.33 \times 10^{-5}$. The *J* and TIP values are consistent with those observed for complex [**7**]$(ClO_4)_2$ and those described in the literature, but the *g* value is too small for a low-spin octahedral Ru(III) complex, for which a value greater than 2 is expected. The failure of the van Vleck equation to yield the expected *g* value points out that the crystal is not purely paramagnetic. Instead, there are intermolecular magnetic interactions along the crystal axes. The *g* value only half as large as expected and the finite extrapolated value of χ_M for $T = 0$ K are indicative of a weak (intermolecular) antiferromagnetic interaction between two dinuclear complexes along at least one of the crystal axes. This interaction is presumably subdued because of increased lattice vibrations at elevated temperature, but it becomes dominant at lower temperatures as evidenced by the sharp drop of μ_{eff} in Figure 2b. The magnetic moment data at 2 K and the apparent *g* value of 1.11 indicate that, at around 0 K, the crystal becomes more or less antiferromagnetic, with an average of one unpaired electron for each dinuclear species.

The pronounced decrease of the magnetic moment with temperature observed in many complexes can also be due to zero-field splitting (ZFS). In many cases, both antiferromagnetic coupling and ZFS are present. The model used in this work considers two Ru(III) centers with one unpaired electron per metal atom ($S = {}^1/_2$). In systems with $S = {}^1/_2$, the ground state cannot be split in the absence of an external magnetic field, and ZFS is not possible. For this reason, in the fit of the magnetic data of complexes **6** and [**7**]$(ClO_4)_2$, ZFS has not been considered. Antiferromagnetic coupling along at least one of the crystal axes emerges as the sole explanation.

(14) Drago, R. S. *Physical Methods for Chemists*, 2nd ed.; Saunders College Publishing: New York, 1992; p 476.

(15) (a) Figgis, B. N.; Reynolds, P. A.; Murray, K. S.; Moubaraki, B. *Aust. J. Chem.* **1998**, *51*, 229. (b) Bendix, J.; Steenberg, P.; Sotofte, I. *Inorg. Chem.* **2003**, *42*, 4510. (c) Barral, M. C.; Jiménez-Aparicio, R.; Pérez-Quintanilla, D.; Priego, J. L.; Royer, E. C.; Torres, M. R.; Urbanos, F. A. *Inorg. Chem.* **2000**, *39*, 65. (d) Jiménez-Aparicio, R.; Urbanos, F. A.; Arrieta, J. M. *Inorg. Chem.* **2001**, *40*, 613. (e) Barral, M. C.; González-Prieto, R.; Jiménez-Aparicio, R.; Priego, J. L.; Torres, M. R.; Urbanos, F. A. *Eur. J. Inorg. Chem.* **2003**, 2339.

(16) Schneider, R.; Weyhermuller, T.; Wieghardt, K.; Nuber, B. *Inorg. Chem.* **1993**, *32*, 4925.

Table 3. Calculated ZINDO/1 Total Energies (in au) for the Monomer and the Dimer of **6**[a]

	monomer		dimer		
spin state	crystallographic geometry[b]	MM+-optimized geometry[c]	sideways[c]	lined-up	sandwiched
singlet	−385.7609	−385.8488	did not converge	−771.4466	did not converge
triplet	−385.7424	−385.8488	−771.7003	did not converge	did not converge
quintet	−385.6368	−385.6959	−771.6977	−771.6058	−771.6152

[a] Convergence limit = 10^{-5} au, iteration limit = 32767. [b] With only the C−H bond lengths optimized by MM+. [c] Whole geometry optimized by MM+.

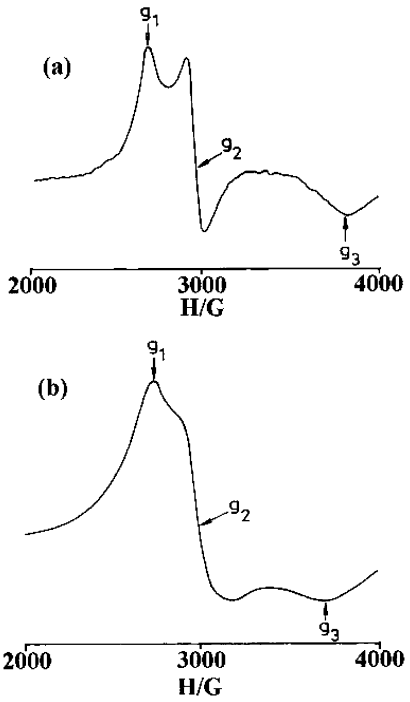

Figure 3. EPR spectra of (a) $[(acac)_2Ru^{III}(\mu\text{-}OC_2H_5)_2Ru^{III}(acac)_2]$, **6**, and (b) $[(acac)_2Ru^{III}(\mu\text{-L})Ru^{III}(acac)_2](ClO_4)_2$, [**7**]$(ClO_4)_2$, in $CHCl_3$ at 77 K.

In this kind of situation, the correct g value for each dinuclear complex would be manifested by EPR in solution. Therefore, we investigated the EPR spectra of samples **6** and [**7**]$(ClO_4)_2$ in the solution phase.

(b) EPR Spectra. 6 and $[\mathbf{7}]^{2+}$ exhibit relatively broad but rhombic EPR spectra in $CHCl_3$ at 77 K (Figure 3), typical of distorted octahedral Ru(III) species[17] ($g_1 = 2.420$, $g_2 = 2.192$, $g_3 = 1.710$ for **6** and $g_1 = 2.385$, $g_2 = 2.177$, $g_3 = 1.753$ for $[\mathbf{7}]^{2+}$). Calculated magnetic moments of 1.85 and 2.20 μ_B at 77 K were obtained for **6** and [**7**]$(ClO_4)_2$, respectively, from the temperature-dependent magnetic moment plots (Figure 2). Average g factors of $\langle g \rangle = 2.128$ and 2.121 for **6** and $[\mathbf{7}]^{2+}$, respectively, were derived from the expression $[^1/_3(g_1^2 + g_2^2 + g_3^2)]^{1/2}$.[18] The solution EPR data reinforce our conclusion that, even though **6** is undoubtedly paramagnetic with a triplet ground state, in the crystal, there must be an antiferromagnetic interaction. Because our conclusion from the studies of the magnetic susceptibility of **6** was supported by the EPR results, we further decided to test the species by semiemperical quantum chemical molecular orbital (MO) calculations.

(c) MO Calculations. The spin states of **6** were scrutinized theoretically by ZINDO/1 method using Hyperchem Professional Release 7.01 software.[19] First, the molecular structure of **6** was obtained from the optimization of each carbon−hydrogen bond length in the crystallographic geometry by the molecular mechanics (MM+) technique. The calculated ZINDO/1 total energy values for different spin states of the optimized structure are reported in Table 3. The singlet emerges as the most stable state, followed by the triplet. The quintet state is the least stable.

Next, the entire molecule was optimized by the MM+ methodology, and the ZINDO/1 calculations were repeated on the optimized geometry. The newly optimized geometry turns out to be more stable than the crystallographic one in each spin state. With this optimized geometry, the singlet and triplet appear to be more or less degenerate (Table 3). This indicates that a higher-level calculation is likely to yield a triplet ground state.

The calculations discussed above indicate the paramagnetic nature of **6** with two unpaired electrons, as observed experimentally. The atomic orbital populations in the triplet reveal that the unpaired electrons are more or less equally and completely localized on the ruthenium atoms in an isolated dinuclear complex.

The spin-state behavior of the dimers of **6** was additionally investigated. These dimer geometries were prepared by placing two complexes with the MM+-optimized geometry for each monomer (**6**) along three orthogonal directions that are approximately along the crystal axes. Thus we obtained the lined-up dimer (**H**), the sideways dimer (**I**), and the sandwiched dimer (**J**). We carried out an MM+ optimization on the sideways dimer. The ZINDO/1 calculations showed that the triplet state is more stable than the quintet by about 1.6 kcal mol^{-1}. This confirms an antiferromagnetic interaction along a direction perpendicular to the dinuclear axis. The singlet-state calculation failed to converge, showing that the singlet is not stable. Hence, the interaction is rather weak. These findings strengthen our conclusion that, along the crystallographic b axis, there exists an antiferromagnetic interaction that leads to an average of one electron per dinuclear complex at around 0 K or an apparent g value half as large as expected.

(17) (a) Chanda, N.; Sarkar, B.; Fiedler, J.; Kaim, W.; Lahiri, G. K. *Dalton Trans.* **2003**, 3550. (b) Samanta, R.; Mondal, B.; Munshi, P.; Lahiri, G. K. *J. Chem. Soc., Dalton Trans.* **2001**, 1827. (c) Mondal, B.; Chakraborty, S.; Munshi, P.; Walawalkar, M. G.; Lahiri, G. K. *J. Chem. Soc., Dalton Trans.* **2000**, 2327. (d) Chakraborty, S.; Walawalkar, M. G.; Lahiri, G. K. *J. Chem. Soc., Dalton Trans.* **2000**, 2875. (e) Munshi, P.; Samanta, R.; Lahiri, G. K. *J. Organomet. Chem.* **1999**, *586*, 176. (f) Santra, B. K.; Menon, M.; Pal, C. K.; Lahiri, G. K. *J. Chem. Soc., Dalton Trans.* **1997**, 1387. (g) Lahiri, G. K.; Bhattacharya, S.; Ghosh, B. K.; Chakravorty, A. *Inorg. Chem.* **1987**, *26*, 4324.

(18) Poppe, J.; Moscherosch, M.; Kaim, W. *Inorg. Chem.* **1993**, *32*, 2640.

(19) *Hyper Chem Professional Release 7 for Windows*; Hypercube Inc.: Gainesville, FL, 2002.

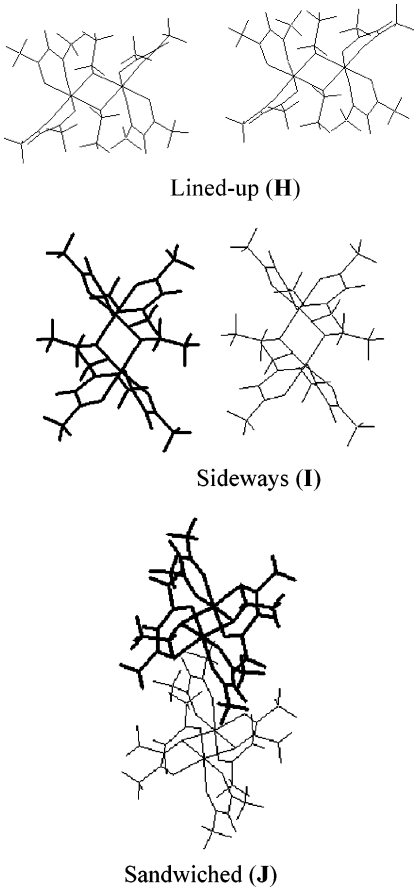

The lined-up and sandwiched dimers were prepared by placing the nearest atoms of the two molecules at a distance that equals the sum of the van der Waals radii of the nearest atoms. In these cases, the calculations on the triplet failed to converge, indicating their relative lack of stability. The quintet states were found to be stable. Hence, ferromagnetic interactions exist along these two directions. Thus ZINDO/1 calculations show the crystal to be overall antiferromagnetic, corresponding to a negative value of θ in eq 2, and of type FAF.

Electron-Transfer Properties. In CH_3CN, **6** exhibits two closely spaced couples with E°_{298},V (ΔE_p, mV) as −0.008-(116) (couple II) and −0.08(65) (couple I) versus SCE (Figure 4a). These are assigned as successive reduction processes involving the metal centers $Ru^{III}Ru^{III} \rightleftharpoons Ru^{III}Ru^{II}$ (couple II) and $Ru^{III}Ru^{II} \rightleftharpoons Ru^{II}Ru^{II}$ (couple I). The separation in potential between the couples is only 70 mV. Therefore, the electrochemical coupling between the metal centers in the mixed-valent state[20] is negligibly small. The low ruthenium(III)−ruthenium(II) reduction potentials (<0.0 V) can account for the preferential stabilization in the Ru(III) state under aerobic condition. The Ru(II)/Ru(III) couples for the corresponding bipyridine derivative $[(bpy)_2Ru^{II}(\mu\text{-}OEt)_2Ru^{II}(bpy)_2]^{2+}$ (**1**) appeared at 0.175 and 0.745 V with a 570-mV potential separation between the stepwise redox processes.[2] Thus, in moving from an electron-rich acetylacetonate environment in **6** to the π-acidic bipyridine ancillary ligand in **1**, a substantial stabilization of the Ru(II) state has taken place as expected.[21] For the catecholato complex $[(Cl_4Cat)_2Ru^{III}(\mu\text{-}OR)_2Ru^{III}(Cl_4Cat)_2]^{4-}$(**2**), however, the successive Ru(III)/(IV) couples were observed at −0.17 and 0.08 V, and the Ru(III)/Ru(II) couple was observed at −1.54 V versus SCE.[3] The observed 570- and 250-mV separations in potentials between the couples in **1** and **2**, respectively, imply the existence of a strong to moderate intermetallic electrochemical coupling in their mixed-valent states.[20] In essence, this coupling leads to the spin pairing of the two ruthenium(III) centers in **2**.[3]

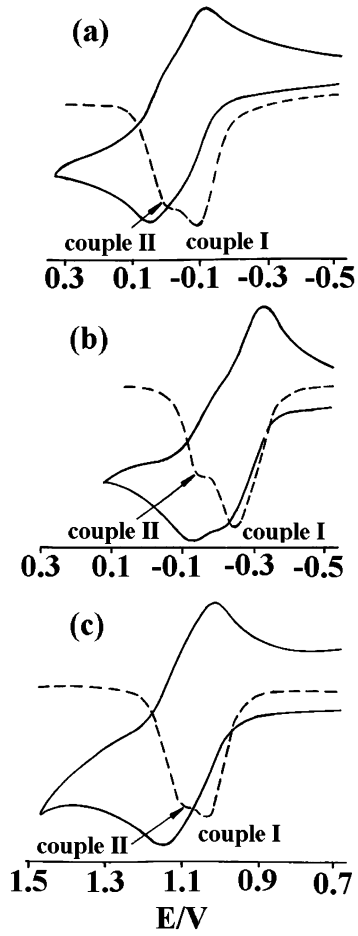

Figure 4. Cyclic voltammograms (—) and differential pulse voltammograms (− − −) of (a) $[(acac)_2Ru^{III}(\mu\text{-}OC_2H_5)_2Ru^{III}(acac)_2]$, **6**; (b) $[(acac)_2Ru^{III}(\mu\text{-}L)Ru^{III}(acac)_2](ClO_4)_2$, $[\mathbf{7}](ClO_4)_2$; and (c) $[(bpy)_2Ru^{II}(\mu\text{-}L)Ru^{II}(bpy)_2](ClO_4)_4$, $[\mathbf{8}](ClO_4)_4$, in CH_3CN.

The two successive quasireversible Ru(III)/Ru(II) couples for the dinuclear complex bridged by L, $[\mathbf{7}]^{2+}$, appear as E°_{298},V (ΔE_p, mV) = −0.15(60) for couple II and −0.26(90) for couple I versus SCE (Figure 4b). However, the differential pulse voltammetric (DPV) current height of couple II is significantly lower than that of couple I (Figure 4b). The partial electrodecomposition into the monometallic fragments might have led to the observed uneven current heights in the two oxidation processes. The separation in potential between the Ru(III)/Ru(II) couples is only 110 mV. Thus, the intermetallic electrochemical coupling in the

(20) (a) Hush, N. S. *Prog. Inorg. Chem.* **1967**, *8*, 391. (b) Robin, M. B.; Day, P. *Adv. Inorg. Radiochem.* **1967**, *10*, 247. (c) Hush, N. S. *Coord. Chem. Rev.* **1985**, *64*, 135.

(21) Chellamma, S.; Lieberman, M. *Inorg. Chem.* **2001**, *40*, 3177.

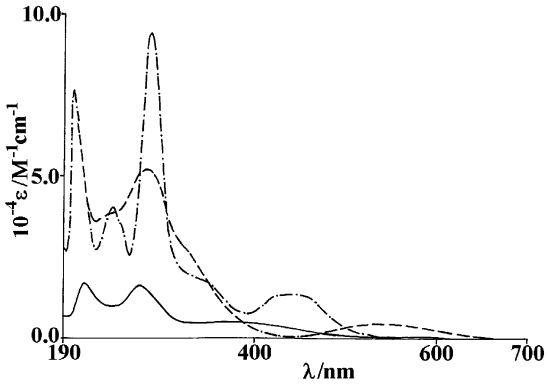

Figure 5. Electronic spectra in CH_3CN of $[(acac)_2Ru^{III}(\mu\text{-}OC_2H_5)_2Ru^{III}(acac)_2]$, **6** (—); $[(acac)_2Ru^{III}(\mu\text{-L})Ru^{III}(acac)_2](ClO_4)_2$, $[\mathbf{7}](ClO_4)_2$ (– – –); and $[(bpy)_2Ru^{II}(\mu\text{-L})Ru^{II}(bpy)_2](ClO_4)_4$, $[\mathbf{8}](ClO_4)_4$ (–•–•–).

mixed-valent state is rather weak, which, in turn, stabilizes $[\mathbf{7}]^{2+}$ in a paramagnetic state. Moreover, this complex also undergoes two irreversible processes at $E_{pa} = 1.51$ and 1.91 V (Supporting Information, Figure S8), which are believed to be due to sequential Ru(III) → Ru(IV) oxidations. The corresponding bipyridine derivative $[\mathbf{8}]^{4+}$ exhibits two closely spaced Ru(III)/Ru(II) couples at E^o_{298},V (ΔE_p, mV) = 1.04(60) for couple I and 1.12(60) for couple II versus SCE, with a separation of 80 mV between the couples, as shown in Figure 4c. The lesser redox stability of Ru(II) state in $[\mathbf{8}]^{4+}$, in comparison to the Ru(II) in $[Ru(bpy)_3]^{2+}$ (E^o, 1.29 V[22]) is clear evidence of the relatively weak ligand field strength of L with respect to bpy. It should be noted that the monomeric form of L, i.e., 2,2′-dipyridylamine also exerts a discernibly weak ligand field strength than the bpy ligand in its ruthenium complexes.[17a] Nevertheless, a potential jump of 1.19 V for the Ru(III)/Ru(II) couple has taken place from the environment of the acac ancillary ligand in $[\mathbf{7}]^{2+}$ to that of bpy in $[\mathbf{8}]^{4+}$. It is obvious that the ruthenium ion in the +3 oxidation state is stabilized in $[\mathbf{7}]^{2+}$. The lack of conjugation in the framework of the bridging ligand L is responsible for the observed weak intermetallic electrochemical coupling in the mixed-valent states of $[\mathbf{7}]^{2+}$ and $[\mathbf{8}]^{4+}$ irrespective of the electronic nature of the ancillary ligands, acac or bpy.[23]

Electrochemically generated mixed-valent species were found to be unstable at room temperature, certainly because of the small separation in potential between the successive couples, which essentially precluded the checking of the electronic and EPR spectra of the mixed-valent congeners.

The reductions of the coordinated bpy moieties in $[\mathbf{8}]^{4+}$ were observed at E^o_{298},V (ΔE_p, mV) = −1.43(60), −1.64(140), and −2.10(190) (Supporting Information, Figure S9).[24]

Electronic Spectra. In acetonitrile, **6** and $[\mathbf{7}]^{2+}$ exhibit three major transitions (Figure 5) (see the Experimental Section). The intense bands in the UV region are characteristic of ligand-centered transitions.[8,25] The expected ligand−metal charge-transfer (LMCT) transitions are observed at 408 and 539 nm for **6** and $[\mathbf{7}]^{2+}$, respectively, as broad absorption bands with comparable intensities.[26] The substantial red shift in the LMCT band energy (>100 nm) on moving from **6** to $[\mathbf{7}]^{2+}$ can be best explained in terms of the relative stabilization of the Ru(III) state in $[\mathbf{7}]^{2+}$ as compared to the alkoxide species, as was observed in their redox potentials.

The bipyridine complex $[(bpy)_2Ru^{II}(\mu\text{-L})Ru^{II}(bpy)_2]^{4+}$, $[\mathbf{8}]^{4+}$, exhibits an MLCT transition at 448 nm with a shoulder at higher energy in addition to the ligand-based transitions that occur in the UV region (Figure 5) (see the Experimental Section).[27] It might be interesting to note that the MLCT band energy of $[\mathbf{8}]^{4+}$ is almost identical to that of the $[Ru(bpy)_3]^{2+}$ complex (450 nm in acetonitrile[22]), although the ligand field strength of the dipyridylamine-based ligand L is expected to be weaker than that of the bpy ligand as reflected in their redox potentials. The separations in potential ($\Delta E_{1/2}$) between the first $Ru^{II} \rightarrow Ru^{III}$ oxidation couple and the first bipyridine reduction in $[\mathbf{8}]^{4+}$ and $[Ru(bpy)_3]^{2+}$ are 2.47 and 2.59 V, respectively. The energies of the MLCT transitions can be predicted with the help of eq 3,[17f,27a] where ν(MLCT) is the predicted wavenumber of the charge-transfer band in cm^{-1}.

$$\nu(\text{MLCT}) = 8065\ (\Delta E_{1/2}) + 3000 \qquad (3)$$

The factor 8065 is used to convert potential in V to cm^{-1}, and the term 3000 cm^{-1} is of an empirical origin. Using the values of 2.47 and 2.59 V for $\Delta E_{1/2}$, the calculated MLCT energies turn out to be 22920 and 23888 cm^{-1} for $[\mathbf{8}]^{4+}$ and $[Ru(bpy)_3]^{2+}$, respectively. These values are in reasonably good agreement with the observed energies, 22321 and 22222 cm^{-1}.

Photophysical Properties. The dinuclear complex $\mathbf{8}^{4+}$ encompassing the bipyridine ancillary function displays a strong emission at 600 nm (Figure 6) with quantum yield $\phi = 0.18$ at 77 K in 4:1 EtOH/MeOH glass. This value is significantly lower than that for $Ru(bpy)_3^{2+}$ ($\phi = 0.34$).[28] Because the emission quantum yield is primarily controlled by the σ-donor strength of the ligand moiety, it might be inferred that the bridging ligand L in $\mathbf{8}^{4+}$ has a weaker ligand field strength than bpy. This is also reflected in their metal redox potentials described earlier. The emission of ruthenium(II) polypyridyl complexes is known to originate from the triplet MLCT state, and so, it is formally phosphorescence. The total emission spectrum of $\mathbf{8}^{4+}$at 77 K is shown in Figure 6a, along with the phosphorescence spectrum in

(22) (a) Alsfasser, R.; Eldik, R. V. *Inorg. Chem.* **1996**, *35*, 628. (b) Coe, B. J.; Meyer, T. J.; White, P. C. *Inorg. Chem.* **1995**, *34*, 593.
(23) Kaim, W.; Klein, A.; Glockle, M. *Acc. Chem. Res.* **2000**, *33*, 755.
(24) (a) Keerthi, K. D.; Santra, B. K.; Lahiri, G. K. *Polyhedron* **1998**, *17*, 1387. (b) Bhattacharya, S. *Polyhedron* **1993**, *12*, 235. (c) Elliott, C. M. *J. Chem. Soc., Chem. Commun.* **1980**, 261. (d) Tokel-Takvoryan, N. E.; Hemingway, R. E.; Bard, A. J. *J. Am. Chem. Soc.* **1973**, *95*, 6583. (e) Morris, D. E.; Hanck, K. W.; DeArmond, M. K. *Inorg. Chem.* **1985**, *24*, 977.
(25) Patra, S.; Sarkar, B.; Mobin, S. M.; Kaim, W.; Lahiri, G. K. *Inorg. Chem.* **2003**, *42*, 6469.
(26) Patra, S.; Miller, T. A.; Sarkar, B.; Niemeyer, M.; Ward, M. D.; Lahiri, G. K. *Inorg. Chem.* **2003**, *42*, 4707.
(27) (a) Sarkar, B.; Laye, R. H.; Mondal, B.; Chakraborty, S.; Paul, R. L.; Jeffery, J. C.; Puranik, V. G.; Ward, M. D.; Lahiri, G. K. *J. Chem. Soc., Dalton Trans.* **2002**, 2097. (b) Chakraborty, S.; Laye, R. H.; Munshi, P.; Paul, R. L.; Ward, M. D.; Lahiri, G. K. *J. Chem. Soc., Dalton Trans.* **2002**, 2348.
(28) (a) Vogler, L. M.; Brewer, K. J. *Inorg. Chem.* **1996**, *35*, 818. (b) Baitalik, S.; Florke, U.; Nag, K. *J. Chem. Soc., Dalton Trans.* **1999**, 719.

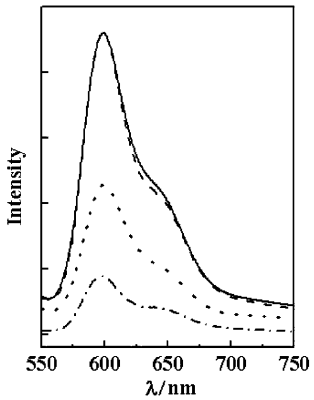

Figure 6. Emission spectra of $\mathbf{8}^{4+}$ at 77 K in 4:1 EtOH/MeOH glass, $\lambda_{ex} = 470$ nm: (a) Total emission spectrum (—), (b) phosphorescence spectrum (delay = 30 μs, gate = 1 ms) (– – –), (c) phosphorescence spectrum (delay = 10 μs, gate = 10 μs) (•••), (d) phosphorescence spectrum (delay = 20 μs, gate = 10 μs) (—•—•—).

Figure 6b. The superimposability of the two spectra confirms that the emission for $\mathbf{8}^{4+}$ is indeed entirely from phosphorescence. However, the radiative lifetime of $\mathbf{8}^{4+}$ is estimated to be ~10 μs from the time evolution of the emission spectra, which is shorter than expected. This is due to the rather strong spin−orbit coupling, which augments the allowedness of the transition. No change in the spectral shape or peak position with the progression of time was observed, unlike the case for the analogous mixed-ligand monomeric complex $Ru(bpy)_2(2,2'\text{-dipyridylamine})^{2+}$, which was observed to exhibit dual emission by De Armond and co-workers.[29] It shows a shorter-lived emission ($\tau_f = 3$ μs) at 640 nm and a longer-lived emission ($\tau_f = 15$ μs) at 590 nm. The lack of such dual emission clearly rules out the existence of multiple emissive states in $\mathbf{8}^{4+}$. Detailed photophysical studies are under way with the aim of rationalizing the difference in behavior of the complexes with monomeric (2,2′-dipyridylamine) and dimeric (L) ligands. In any case, $\mathbf{8}^{4+}$ is a highly promising emissive probe with interesting excited-state properties.

Conclusions

The present work illustrates the following important features: (1) The new dialkoxo-bridged paramagnetic diruthenium(III) complex $(acac)_2Ru^{III}(\mu\text{-}OC_2H_5)_2Ru^{III}(acac)_2$, **6**, has been prepared. (2) The paramagnetic and diamagnetic diruthenium complexes bridged by *N*,*N*,*N*′,*N*′-tetra(2-pyridyl)-1,4-phenylenediamine (L) $[(acac)_2Ru^{III}(\mu\text{-L})Ru^{III}(acac)_2](ClO_4)_2$, $[\mathbf{7}](ClO_4)_2$, and $[(bpy)_2Ru^{II}(\mu\text{-L})Ru^{II}(bpy)_2](ClO_4)_4$, $[\mathbf{8}](ClO_4)_4$, respectively, have been synthesized. (3) Diruthenium complexes **6**, $[\mathbf{7}]^{2+}$, and $[\mathbf{8}]^{4+}$ exhibit negligible intermetallic electrochemical coupling in their mixed-valent states, as evidenced by cyclic voltammetry. (4) Paramagnetic complexes **6** and $[\mathbf{7}]^{2+}$ display rhombic EPR spectra corresponding to the distorted octahedral Ru(III) ion. The species **6** is especially interesting as the temperature dependence of the magnetic susceptibility yields a *g* value only half as large as the expected value, whereas the solution EPR gives a *g* value in the correct range. We interpret this feature as arising from a weak antiferromagnetic interaction along one of the crystal axes, for which we garner further support from theoretical calculations. A more in-depth theoretical analysis is necessitated. (5) The bipyridine derivative $[\mathbf{8}]^{4+}$ exhibits unusually strong luminescence having a quantum yield (ϕ) = 0.18 and an estimated excited-state lifetime of about 10 μs.

Experimental Section

The starting complexes *cis*-$[Ru(acac)_2(CH_3CN)_2]$ and *cis*-$[Ru(bpy)_2(EtOH)_2]^{2+}$ were prepared according to the reported procedures.[30,31] The dinucleating bridging ligand *N*,*N*,*N*′,*N*′-tetra(2-pyridyl)-1,4-phenylenediamine $[(NC_5H_4)_2{-}N{-}C_6H_4{-}N{-}(NC_5H_4)_2$ (L)] was synthesized by following the literature procedure.[8] The compound 2,2′-dipyridylamine was purchased from Aldrich. Other chemicals and solvents were of reagent grade and were used as received. For electrochemical studies, HPLC-grade acetonitrile was used. Commercial tetraethylammonium bromide was converted to pure tetraethylammonium perchlorate (TEAP) by following an available procedure.[32] The electrical conductivity of the solution was checked using a Systronic conductivity bridge 305. Infrared spectra were taken on a Nicolet spectrophotometer with samples prepared as KBr pellets. The ^{1}H NMR spectrum was obtained on a 300-MHz Varian FT-NMR spectrometer. UV−visible spectra were recorded on a Jasco-570 spectrophotometer. Cyclic voltammetry and coulometric measurements were carried out using a PAR model 273A electrochemistry system. A platinum working electrode, a platinum wire auxiliary electrode, and a saturated calomel reference electrode (SCE) were used in a three-electrode configuration. Tetraethylammonium perchlorate (TEAP) was the supporting electrolyte, and the concentration of the solution was 10^{-3} M. The half-wave potential E^0_{298} was set equal to $0.5(E_{pa} + E_{pc})$, where E_{pa} and E_{pc} are the anodic and cathodic cyclic voltammetric peak potentials, respectively. The scan rate used was 50 mV s^{-1}. A platinum gauze working electrode was used in coulometric experiments. All electrochemical experiments were carried out under a dinitrogen atmosphere and are uncorrected for junction potentials. The elemental analyses were carried out using a Perkin-Elmer 240C elemental analyzer. Emission experiments were made using a Perkin-Elmer LS 55 spectrometer fitted with a cryostat, and the quantum yield (ϕ) was determined by following a previously described method.[11a,22a] Electrospray mass spectra were recorded on a Micromass Q-TOF mass spectrometer. The variable-temperature magnetic susceptibility data were measured on a Quantum Design MPMSXL SQUID (Superconducting Quantum Interference Device) susceptometer over a temperature range of 2−300 K. Each raw data field was corrected for the diamagnetic contributions of both the sample holder and the complex to the susceptibility. The molar diamagnetic corrections for the complexes were calculated on the basis of Pascal constants. The fitting of the experimental data was carried out using the commercial MATLAB V.5.1.0.421 program.

Caution! Perchlorate salts of metal complexes are potentially explosive. Care should be taken while handling such complexes.

(29) (a) Blakley, R. L.; Myrick, M. L.; DeArmond, M. K. *J. Am. Chem. Soc.* **1986**, *108*, 7843. (b) Blakley, R. L.; DeArmond, M. K. *J. Am. Chem. Soc.* **1987**, *109*, 4895.

(30) Kasahara, Y.; Hoshino, Y.; Shimizu, K.; Sato, G. P. *Chem. Lett.* **1990**, 381.

(31) (a) Kar, S.; Miller, T. A.; Chakraborty, S.; Sarkar, B.; Pradhan, B.; Sinha, R. K.; Kundu. T.; Ward, M. D.; Lahiri, G. K. *Dalton Trans.* **2003**, 2591. (b) Sullivan, B. P.; Salmon, D. J.; Meyer, T. J. *Inorg. Chem.* **1978**, *17*, 3334.

(32) Sawyer, D. T.; Sobkowiak, A.; Roberts, J. L., Jr. *Electrochemistry for Chemists*; Wiley: New York, 1995.

Synthesis of 6 and [7](ClO$_4$)$_2$. The dinucleating bridging ligand $(NC_5H_4)_2-N-C_6H_4-N-(NC_5H_4)_2$ (L) (54 mg, 0.13 mmol) was added to the starting complex *cis*-[Ru(acac)$_2$(CH$_3$CN)$_2$] (100 mg, 0.26 mmol) in ethanol (20 mL). The resulting mixture was heated to reflux under aerobic conditions for 12 h. The solvent was then removed under reduced pressure. The solid mass thus obtained was purified using a silica gel column. The complexes **6** and [**7**](ClO$_4$)$_2$ were eluted by 10:1 CH_2Cl_2/CH_3CN and $NaClO_4$ solution in CH_3CN, respectively. The complexes **6** and [**7**](ClO$_4$)$_2$ were then recrystallized from dichloromethane/hexane (1:1) and acetonitrile/benzene (1:4), respectively.

For **6**: Yield 20% (18 mg). Anal. Calcd (found) for $C_{24}H_{38}O_{10}Ru_2$ (**6**): C, 41.86 (41.59); H, 5.56 (5.80). λ_{max}, nm (ϵ, M^{-1} cm^{-1}): 408 (4770), 376 (5280), 276 (16074), 214 (16980).

For [**7**](ClO$_4$)$_2$: Yield 50% (81 mg). Anal. Calcd (found) for $C_{46}H_{48}N_6Cl_2O_{16}Ru_2$ {[**7**](ClO$_4$)$_2$}: C, 45.51 (45.69); H, 3.99 (3.68); N, 6.92 (7.12). Molar conductivity [Λ_M (Ω^{-1} cm^2 mol^{-1})] in acetonitrile: 226. λ_{max}, nm (ϵ, M^{-1} cm^{-1}): 539 (4530), 326 (27400), 282 (51970), 241 (38361), 203 (76360).

Synthesis of [8](ClO$_4$)$_4$. The starting complex *cis*-Ru(bpy)$_2$Cl$_2$·2H$_2$O (100 mg, 0.19 mmol) and $AgClO_4$ (85 mg, 0.39 mmol) were taken in ethanol (15 mL), and the mixture was heated to reflux with stirring for 1.5 h. The initial violet solution was changed color to orange-red. It was then cooled and filtered through a sintered glass funnel (G-4). The ligand (L) (40 mg, 0.095 mmol) was then added to the above [Ru(bpy)$_2$(EtOH)$_2$]$^{2+}$solution. The resulting mixture was heated to reflux under aerobic conditions for 12 h. The precipitate that formed upon cooling was filtered and washed thoroughly with ice-cold water followed by cold ethanol and diethyl ether. The solid mass thus obtained was then purified by using an alumina column (neutral). The complex [**8**](ClO$_4$)$_4$ was eluted by 1:1 CH_2Cl_2/CH_3CN. The product was recrystallized from acetonitrile/benzene (1:6). Yield 54% (85 mg). Anal. Calcd (found) for $C_{66}H_{52}N_{14}Cl_4O_{16}Ru_2$ {[**8**](ClO$_4$)$_4$}: C, 48.30 (48.73); H, 3.19 (3.56); N, 11.95 (11.75). Molar conductivity [Λ_M (Ω^{-1} cm^2 mol^{-1})] in acetonitrile: 460. λ_{max}, nm (ϵ, M^{-1} cm^{-1}): 448 (13524), 336 (18690), 289 (94031), 245 (39970), 204 (68760).

Crystal Structure Determination. Single crystals of L were grown by slow diffusion of a dichloromethane solution of L in hexane followed by slow evaporation. Single crystals of **6** were grown by slow diffusion of an acetonitrile solution of **6** in benzene followed by slow evaporation. X-ray data of L and **6** were collected on a PC-controlled Enraf-Nonius CAD-4 (MACH-3) single-crystal X-ray diffractometer using Mo Kα radiation. Crystal data and data collection parameters are listed in Table 1. The structures were solved and refined by full-matrix least-squares on F^2 using SHELX-97 (SHELXTL).[33] Hydrogen atoms were included in the refinement process as per the riding model.

Acknowledgment. We thank the Council of Scientific and Industrial research, New Delhi, India, for financial support. The X-ray structural studies were carried out at the National Single Crystal Diffractometer Facility, Indian Institute of Technology, Bombay, India. Special acknowledgment is made to the Sophisticated Analytical Instrument Facility, Indian Institute of Technology, Bombay, India, for providing the NMR and EPR facilities. We are grateful to S. N. Datta and P. Jha for help in calculations involving Hyperchem Professional Release.

Supporting Information Available: X-ray crystallographic data for L and **6** in CIF format; electrospray mass spectra of **6** (Figure S1), [**7**](ClO$_4$)$_2$ (Figure S2), and [**8**](ClO$_4$)$_4$ (Figure S3); ^{1}H NMR spectrum of [**8**](ClO$_4$)$_4$ (Figure S4); ORTEP diagram of L (Figure S5); packing diagrams of **6** (Figure S6); plots of the reciprocal of the magnetic susceptibility versus temperature for [**7**](ClO$_4$)$_2$ and (**6**) (Figure S7); cyclic and differential pulse voltammograms of [**7**](ClO$_4$)$_2$ (Figure S8); cyclic and differential pulse voltammograms of [**8**](ClO$_4$)$_4$ (Figure S9); selected bond distances (Å) and angles (deg) for L (Table S1). This material is available free of charge via the Internet at http://pubs.acs.org.

IC0498900

(33) Sheldrick, G. M. *SHELX-97 Program for Crystal Structure Solution and Refinement*; University of Göttingen, Göttingen, Germany, 1997.